Photoacoustic Blood Oxygenation Imaging Based on Semiconductor Lasers

Claus-Stefan Friedrich[1], Martin P. Mienkina[2], Carsten Brenner[1], Nils C. Gerhardt[1], Manfred Jörger[3], Andreas Strauß[3], Martin F. Beckmann[2], Georg Schmitz[2], Martin R. Hofmann[1]

[1]Photonics and Terahertz-Technology, Ruhr-Universität Bochum, 44801 Bochum, Germany

[2]Institute of Medical Engineering, Ruhr-Universität Bochum, 44801 Bochum, Germany

[3]ILIAS-medical GmbH, 44799 Bochum, Germany

[1]claus-stefan.friedrich@rub.de

***Abstract*-- We present a multi-wavelength semiconductor laser system in combination with a standard clinical ultrasound system for photoacoustic blood oxygenation imaging. We demonstrate its ability to measure blood oxygenation quantitatively. To model human whole blood properties we used porcine whole blood samples. The resulting oxygenation values are in good agreement with the values obtained by a commercially available blood oxygenation measurement system (R^2=0.96) over a wide range of oxygen saturations. By using a blood vessel mimicking sample we demonstrate quantitative spatially resolved oxygenation imaging.**

***Keywords*-- Semiconductor Lasers; Photoacoustic Imaging; Blood oxygenation; Multi-wavelength Semiconductor Laser System**

I. INTRODUCTION

Non-invasive spatially resolved blood oxygenation imaging of subcutaneous blood vessels would be a valuable tool for monitoring wound healing [1], brain injuries [2] or for functional brain imaging [3]. This can be done by multi-wavelength photoacoustic imaging. As has already been shown in [4], photoacoustic imaging allows for imaging of cerebral structures. Laufer et al. [5,6], demonstrated *in vitro* oxygenation measurements by using a saline suspension of red blood cells. Petrova et al. [7] presented *in vivo* blood oxygenation determination within the superior sagittal sinus of a sheep. Unfortunately, this new biomedical imaging technique still suffers from the need of expensive and bulky Nd:YAG-lasers in combination with Optical-Parametric-Oscillators (Nd:YAG-OPO). We present a compact and cost effective semiconductor laser based multi-wavelength photoacoustic system as an alternative. Semiconductor lasers exhibit lower pulse energies than their bulky competitors, but this drawback can be compensated by coded excitation techniques as has been reported in [8] and [9].

First experiments of Kolkman et al. [10] and Allen et al. [11] already showed that semiconductor lasers are able to generate photoacoustic signals in blood vessels and allow for qualitative oxygen saturation measurements. Kolkman et al. [10] demonstrated how blood can be used as natural contrast agent for *in vivo* spatially resolved subcutaneous vessel imaging, but did not encounter any blood oxygenation measurements. Within their experiment the spatially resolved image was generated by scanning a custom made single element transducer across the investigated blood vessel. Allen et al. [11] presented *in vivo* qualitative oxygenation measurements without spatial resolution employing also a single element transducer.

Because of their high sensitivity single element transducers might be the best choice to detect photoacoustic signals excited by semiconductor lasers, but for photoacoustic imaging ultrasound transducer arrays would be easier to use. However, these arrays are commonly less sensitive than single element transducers. Therefore the scope of this study is to document the ability of semiconductor laser based photoacoustic systems to allow for quantitative oxygen saturation determination in general, and even quantitative oxygenation imaging by using a standard ultrasound transducer array.

In this article we present a four wavelength semiconductor laser system to demonstrate quantitative photoacoustic blood oxygenation measurements *in vitro* using porcine whole blood as a model of human blood.

In section II.A we describe the model we used to photoacoustically determine the oxygen saturation. This section is followed by a description of the reference system. Then we motivate the use of porcine blood and describe the sample generation. After presenting the experimental setups we explain our calibration sequence. The last part includes the experimental results followed by a conclusion.

II. METHODS AND MATERIALS

A. Photoacoustic Detection Model

Photoacoustic imaging is based on the photoacoustic effect. According to [12, 13], the generated photoacoustic signal can be derived from the following quasi-stationary equation:

$$p_{gen} = \Gamma \mu_a \eta_{th} F \qquad (1)$$

In Eq. (1), p_{gen} defines the initial pressure amplitude, Γ is the Grüneisen parameter, μ_a is the optical absorption coefficient of the sample, η_{th} is the heat conversion efficiency factor and F the incident fluence of the laser beam. This equation shows that the photoacoustic signal is directly proportional to the optical absorption coefficient of the illuminated material. Spectrally differently absorbing materials can be separated, for example, by using multi-wavelength laser sources.

Photoacoustic blood oxygenation imaging is based on the different molar extinction coefficients of oxygenated and deoxygenated hemoglobin at certain wavelengths. A simple

approach to determine the concentration of each hemoglobin compound, as, for instance, mentioned in [5], can be derived by using the following relation between the absorption coefficient and the molar extinction coefficients ε_{HbO_2} and ε_{Hb} of oxygenated and deoxygenated hemoglobin, respectively:

$$\mu_a(\lambda_i) = \ln(10)\cdot\left(c_{HbO_2}\cdot\varepsilon_{HbO_2}(\lambda_i) + c_{Hb}\cdot\varepsilon_{Hb}(\lambda_i)\right) = K_{HbO_2}\cdot\varepsilon_{HbO_2}(\lambda_i) + K_{Hb}\cdot\varepsilon_{Hb}(\lambda_i) \quad (2)$$

Here, c_{HbO_2} and c_{Hb} are the concentrations of oxygenated and deoxygenated hemoglobin. K_{Hb} and K_{HbO_2} can be used to derive the oxygen saturation $SatO_2$ which is defined as

$$SatO_2 = \frac{c_{HbO_2}}{c_{Hb}+c_{HbO_2}}\cdot 100\% = \frac{K_{HbO_2}}{K_{Hb}+K_{HbO_2}}\cdot 100\% \quad (3)$$

Eq. (1) can be transformed by using Eq. (2) into:

$$p_{gen} = \Gamma\cdot\left(K_{HbO_2}\cdot\varepsilon_{HbO_2}(\lambda_i) + K_{Hb}\cdot\varepsilon_{Hb}(\lambda_i)\right)\cdot\eta_{th}\cdot F \quad (4)$$

Eq. (4) describes the generation of the photoacoustic pressure amplitude p_{gen}. The measured photoacoustic amplitude is somewhat different: According to [14] the detected photoacoustic signal consists of three principle factors: A fluence factor describing the properties of the optical source, a sample factor describing the sample's optical and acoustical behavior and a transfer function factor describing the system dependent response.These contributions are discussed in more detail in the following:

1) Fluence Factor:

The fluence factor is represented in Eq. (4) by the fluence F. Eq. (4) expects F to be constant and especially not to be a function of the wavelength λ_i. For our multi-wavelength semiconductor laser system this might not be the case: It consists of different laser diodes emitting different laser beam profiles which will result in different intensity distributions. In addition, the laser diode beams are often focused to increase the intensity resulting in different spot sizes. Therefore a wavelength dependent correction factor $N(\lambda_i)$ has to be included.

Furthermore, Eq. (4) is only valid for non-scattering materials. As has been demonstrated in [15], whole blood is a scattering material. Moreover, the scattering itself also depends on the wavelength and the oxygen saturation of the blood. The scattering produces a subsurface increase in optical intensity as the photons remain in the adjacent region below the blood surface for a longer time which results in a larger number of absorbing events. Eq. (4) therefore has to be changed to ([16])

$$p_{gen} = \Gamma\cdot\left[M_{HbO_2}(\lambda_i)\cdot K_{HbO_2}\cdot\varepsilon_{HbO_2}(\lambda_i) + M_{Hb}(\lambda_i)\cdot K_{Hb}\cdot\varepsilon_{Hb}(\lambda_i)\right]\cdot N(\lambda_i)\cdot\eta_{th}\cdot F \quad (5)$$

$M_{HbO_2}(\lambda_i)$ and $M_{Hb}(\lambda_i)$ model the changes due to scattering of the photoacoustic pressure amplitude.

As has been described in [16], the increase of the detected photoacoustic signal due to scattering can be observed at light penetration depths larger than the effective light penetration depth $\frac{1}{\mu_{eff}}$. μ_{eff}, the effective attenuation coefficient, is defined as:

$$\mu_{eff}(\lambda_i) = \sqrt{3\cdot\mu_a(\lambda_i)\cdot\left(\mu_a(\lambda_i) + g\mu_s(\lambda_i)\left(1 - g(\lambda_i)\right)\right)} \quad (6)$$

Here, $\mu_s(\lambda_i)$ is the scattering coefficient and $g(\lambda_i)$ is the anisotropy factor of the blood. As has been demonstrated in [14] the acoustic spectrum can be used to determine the influence of the scattering on the photoacoustic signal. Unfortunately, this approach requires a broad bandwidth ultrasound transducer. The bandwidths of the standard transducers employed within this study are too limited and the generated photoacoustic signal has been too weak to apply this approach.

2) Acoustical and Optical Properties:

The sample's acoustical and optical properties are modeled in Eq. (5) by the Grüneisen coefficient Γ and the optical absorption coefficient expressed in terms of the molar extinction coefficients ε_{HbO_2} and ε_{Hb}. This simple approach is only valid under ideal circumstances: It assumes that oxygenated and deoxygenated hemoglobin are the only absorbing materials within the sample. Other hemoglobin derivatives, like for instance methemoglobin and any other absorbing constituents of the blood, are not considered. According to [5], apart from water absorption other absorbing substances within the blood sample can be neglected. The absorption coefficient of water (as has been reported in [17]) within the wavelength range from 650nm to 905nm is at least 50 times lower than the absorption of the hemoglobin derivatives assuming a minimal hemoglobin concentration in porcine blood of 6.8 mmol/L ([18]). Especially at 650nm, where the difference between the extinction coefficients of oxygenated and deoxygenated hemoglobin is very pronounced, the water absorption is more than 500 times lower than the absorption of the corresponding hemoglobin derivatives. Therefore water absorption can be neglected in the following.

3) Transfer Function:

The influence of the sytem's transfer function on the detected photoacoustic signal can be reduced to a simple factor Q if the amplitude of the demodulated acoustical signal is used (absolute value of the analytic signal) and if we assume linear acoustic behavior:

$$p(\lambda_i) = Q\cdot\left[\Gamma\cdot\left(M_{HbO_2}(\lambda_i)\cdot K_{HbO_2}\cdot\varepsilon_{HbO_2}(\lambda_i) + M_{Hb}(\lambda_i)\cdot K_{Hb}\cdot\varepsilon_{Hb}(\lambda_i)\right)\cdot N(\lambda_i)\cdot\eta_{th}\cdot F\right] \quad (7)$$

We did not use flowing blood during our experiments, therefore $M_{HbO_2}(\lambda_i)$ and $M_{Hb}(\lambda_i)$ are potentially additionally influenced by sedimentation. Hence, for a quantitative measurement of the oxygen saturation, the unknown parameters $M_{HbO_2}(\lambda_i)$ and $M_{Hb}(\lambda_i)$ have to be determined within a calibration sequence. Afterwards, Eq. (7) can be used to form a system of equations by using different wavelengths

and K_{Hb} and K_{HbO_2} can be determined by a pseudo-inverse matrix technique to be able to calculate $SatO_2$ from Eq. (3).

If the light penetration depth is lower than the effective light penetration depth due to the blood sample geometry, Eq. (7) reduces to

$$p(\lambda_i) = Q \cdot \left[\Gamma \cdot \left(K_{HbO_2} \cdot \varepsilon_{HbO_2}(\lambda_i) + K_{Hb} \cdot \varepsilon_{Hb}(\lambda_i) \right) \cdot N(\lambda_i) \cdot \eta_{th} \cdot F \right] \quad (8)$$

B. Porcine Whole Blood Model

We used porcine whole blood to model human blood. Porcine blood is easier to obtain in sufficient amounts and there are less strict handling restrictions. According to [19] the optical behavior of porcine and human hemoglobin is quite similar. We used the molar extinction coefficients for porcine hemoglobin listed in [19] for the photoacoustic determination of the oxygen saturation values.

Using whole blood samples is more realistic than using hemoglobin dilutions: Within whole blood the hemoglobin molecules are contained in red blood cells (RBC) and, according to [15], the difference between the refractive indices of the RBCs and the surrounding blood plasma results in optical scattering. Therefore the optical scattering behavior would differ from *in vivo* measurements if only hemoglobin dilutions were used. Even red blood cell dilutions might show different optical and acoustical behavior compared to whole blood, because other blood particles may also influence the measured photoacoustic signal.

C. Reference System

In order to demonstrate the accuracy of our photoacoustic oxygen saturation detection system a reference system is necessary. The reference system we used was an IRMA TruPoint Blood Analysis System(R) which measures the partial pressure of Oxygen $pO_{2,S}$, the partial pressure of carbon dioxide $pCO_{2,S}$ and the pH value at a temperature T of 37°C. To determine the oxygen saturation from the partial oxygen pressure pO_2 at standard conditions we use the standard porcine oxygen dissociation curve presented in [20]:

$$SatO_{2,ref} = \frac{(0.13534 \cdot pO_2)^{3.02}}{(0.13534 \cdot pO_2)^{3.02} + 91.2} \quad (9)$$

The oxygen dissociation curve represents the binding properties of hemoglobin by relating the partial oxygen pressure to the oxygen saturation which describes the oxygen bound to hemoglobin. Although porcine blood shows similar optical behavior the oxygen dissociation curve of porcine hemoglobin differs significantly from human hemoglobin. That is why a standard porcine oxygen dissociation curve has to be used. This standard oxygen dissociation curve is only valid for $pH = 7.4$, $pCO_2 = 40\text{mmHg}$ and $T = 37°C$. For measurements, with different pH - and pCO_2 -values, the oxygen dissociation curve is shifted to higher or lower partial oxygen pressures. To be able to use the standard oxygen dissociation curve, it has to be accounted for these shifts.

According to [21], the shift for porcine blood due to a pH change can be derived by multiplying the measured partial pressure by an empirical factor. For human blood the pCO_2 -changes can be modeled by another empirical factor [22]. Here we presume a similar behavior for porcine blood. The modified partial oxygen pressure, which is used to calculate the oxygen saturation, is therefore

$$pO_2 = pO_{2,S} \cdot 10^{-0.441(7.4-pH)} \cdot 10^{0.06\left(\log_{10}(40) - \log(pCO_{2,S})\right)} \quad (10)$$

A temperature correction of the oxygen saturation is not necessary according to [23] and [24]. Its temperature dependence is, in contrast to the influence on the partial oxygen pressure, negligible over a wide temperature range. Therefore, $SatO_{2,ref}$ is considered to remain constant during the optical measurements. The oxygen saturation values obtained by this procedure are afflicted by a maximum relative error of 6-13% (below $SatO_{2,ref} = 85\%$: 13%, above: 6%) due to uncertainties of the three measured parameters and the correction factors. This results, for instance, in a maximum absolute uncertainty of the oxygen saturation value of $\Delta SatO_{2,ref} = \pm 5.4\%$ at a saturation level of $SatO_{2,ref} = 90\%$ for the reference system.

D. Sample Preparation

Fresh porcine blood was obtained from a slaughterhouse and stabilized with Heparin (Heparin-Natrium-5000 ratiopharm, 5000 i.u. / 0.2ml solution per 1 liter porcine blood). It was completely deoxygenated by using nitrogen. Afterwards the blood was oxygenated within an artificial blood circuit by a MEDOS HILITE 7000 oxygenator (MEDOS Medizintechnik AG, Germany) up to various saturation levels. The resulting blood samples were stored in syringes. Within the first setup OptiCell(TM) sample containers were used for each blood sample. The partial oxygen pressure measurement was performed twice, directly before filling the OptiCell(TM) and after the photoacoustic measurements. The resulting partial oxygen pressure did not differ significantly before and after the photoacoustic measurements.

In the second setup for quantitative spatially resolved oxygen saturation measurements we used two PVC-hoses with an inner diameter of approximately 0.45mm. Firstly, both tubes were filled with the same porcine blood sample and secondly the blood sample was changed in one of them.

III. Setup Description

The experimental setups we used are shown in Fig. 1 and Fig. 2. The photoacoustic signal is obtained in transmission geometry.

The semiconductor laser source consisted of four different semiconductor lasers with four different wavelengths (650nm, 19 emitter custom made by Ferdinand-Braun-Institut für Höchstfrequenztechnik, Germany; 808nm, JOLD-225-QPFN-1L 808, Jenoptik, Germany; 850nm, CVD 197-90-00, LDI, USA; 905nm, 905D3S3J08U, Laser Components, Germany) which are coupled into a 600µm-core fiber bundle. The semiconductor lasers are used in pulse operation mode with a pulse width of 100ns and a repetition frequency of 1041Hz. The emitted pulse energies are approximately 8.5µJ at 650nm, 5.5µJ at 808nm, 5µJ at 850nm and 12µJ at 905nm. To

optimize the generated photoacoustic signal, the laser light is focused on the sample. The generated acoustic signal is detected by a single element transducer (Olympus Panametrics-C380, center frequency: 3.5 MHz, focal length: 75 mm) combined with a cascade of two amplifiers (Miteq AU-3A-0110, 58dB and Olympus Panametrics NDT 5900PR) in the first setup or by a curved transducer array (C5-2/60, Ultrasonix Medical Corp., Canada, nominal center frequency: 3.5 MHz) combined with a modified clinical ultrasound system (Sonix RP, Ultrasonix Medical Corp.) in the second setup.

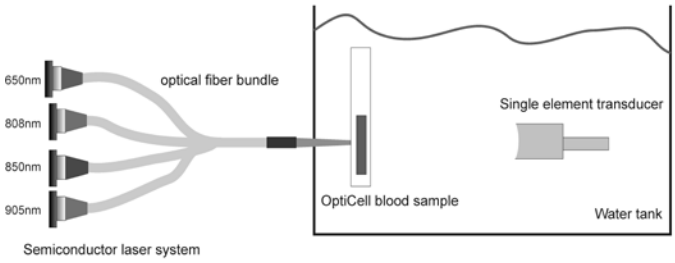

Fig. 1 Setup 1: OptiCell blood sample detected by single element transducer.

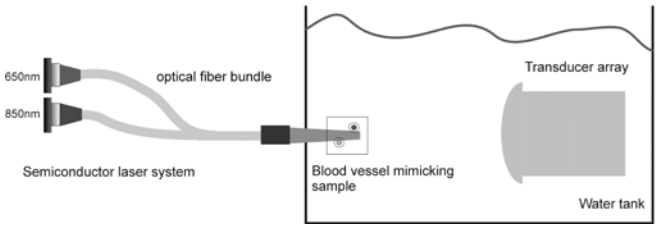

Fig. 2 Setup 2: Blood vessel mimicking sample detected by transducer array.

We use two different setups. The first one (Fig. 1) consists of the OptiCell(TM)-sample which is illuminated by the described semiconductor laser system and the resulting photoacoustic signal is detected by the single element transducer. This setup was used to demonstrate the principle ability of the system to measure oxygen saturation quantitatively. The calibration was done within the same geometry.

To demonstrate the system's capability of the spatially resolved quantitative oxygen saturation determination, we exchanged the OptiCell(TM)-sample by the blood vessel mimicking sample (two PVC-hoses placed in water, inner diameter: approximately 0.45mm, Fig. 2). For spatially resolved oxygenation imaging it is necessary that the illumination patterns of all laser beams are equal. This could be realized for two different wavelengths only within this setup. In this setup the single element transducer was replaced by the curved transducer array.

IV. Calibration Sequence

The calibration sequence can be subdivided into two parts: First, the obtained photoacoustic signal has to be normalized to the incident optical intensity for each wavelength. This is done by photoacoustically measuring a neutral density filter (NG9, Schott AG, Germany) within the used setup. The photoacoustic signal is divided by the known optical absorption of the filter and the result is used as a normalizing divisor. In this way, the wavelength dependent factor $N(\lambda_i)\cdot\eta_{th}\cdot F$ can be eliminated.

If it is necessary to account for scattering influences on the photoacoustic signal, the parameters $M_{HbO_2}(\lambda_i)$ and $M_{Hb}(\lambda_i)$ have to be determined within a second step by using two blood samples with different oxygen saturation values. Within this calibration step a system of two equations for each wavelength based on Eq. (7) is built to determine two unknown virtual parameters $\eta_{Hb}(\lambda_i)$ and $\eta_{HbO_2}(\lambda_i)$ by the known parameters $p(\lambda_i)$, K_{Hb} and K_{HbO_2} (indirectly by using $SatO_2$). $\eta_{Hb}(\lambda_i)$ and $\eta_{HbO_2}(\lambda_i)$ are defined as

$$\eta_{Hb}(\lambda_i) = Q\cdot\Gamma\cdot M_{Hb}(\lambda_i) \tag{11}$$

$$\eta_{HbO_2}(\lambda_i) = Q\cdot\Gamma\cdot M_{HbO_2}(\lambda_i) \tag{12}$$

Therefore $M_{HbO_2}(\lambda_i)$ and $M_{Hb}(\lambda_i)$ are only indirectly determined by this calibration sequence. Best results are obtained by using one almost completely deoxygenated and one almost completely oxygenated blood sample of known oxygen saturation. This lowers the influence of measurement errors on the calibration parameters.

V. Experimental Results

Using the first experimental setup, Fig. 3 and Fig. 4 show the dependency of the measured photoacoustic signal amplitude on the oxygen saturation values determined by the reference system. The photoacoustic signal amplitude has been normalized to the incident optical intensity (first calibration step). The photoacoustic signal amplitude has been obtained by averaging (1000 times) and demodulating the transducers voltage signal by using the absolute value of the analytical signal.

If we assume that the total hemoglobin content remains constant for all blood samples, the sum $K = K_{HbO_2} + K_{Hb}$ also remains constant and Eq. (7) can be changed into

$$p(\lambda_i) = Q\cdot\Gamma\cdot N(\lambda_i)\cdot\eta_{th}\cdot F\cdot K\cdot\left[\left(M_{HbO_2}(\lambda_i)\cdot\varepsilon_{HbO_2}(\lambda_i) - M_{Hb}(\lambda_i)\cdot\varepsilon_{Hb}(\lambda_i)\right)\cdot SatO_2 + \frac{M_{Hb}(\lambda_i)\cdot\varepsilon_{Hb}(\lambda_i)}{K}\right] \tag{13}$$

In theory the photoacoustic signal amplitude therefore depends linearly on the oxygen saturation value. This theoretical linear dependency has been fitted to the experimental values obtained for the excitation wavelengths 650nm, 808nm, 850nm and 905nm. The results are illustrated in Fig. 3 and Fig. 4. Please note that the data shown in Fig. 3 and Fig. 4 are not calibrated. The uncertainties of the reference system are also depicted to define the accuracy limits of this measurement. The coefficient of determination R^2 of this fitting is highly wavelength dependent: The best linear behavior is obtained at an excitation wavelength of 650nm (R^2=0.94) whereas the near infrared wavelengths show less agreement with the theory (808nm: R^2=0.43, 850nm: R^2=0.80, 905nm: R^2=0.70). These differences to the theoretical linear behavior result, most probably, from the combination of low light pulse energies of the exciting lasers

with low differences in the optical absorption between the two hemoglobin derivatives at the regarded wavelength. In addition to this the wavelength dependent scattering coefficient of blood may also cause a higher signal-to-noise ratio at 650nm than at any near infrared wavelength. The higher scattering coefficient at 650nm produces a subsurface increase in optical intensity as the photons remain in the adjacent region below the blood surface for a longer time. This results in a larger number of absorbing events and a stronger photoacoustic signal ([15], [16]). Both effects lead to a stronger scattering of the photoacoustic measurement data for near infrared wavelengths. According to this explanation visible light emitting laser diodes, like the 650nm semiconductor laser, are necessary for accurate oxygen saturation measurements.

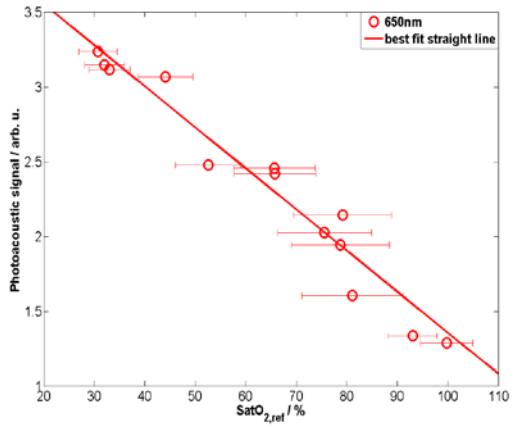

Fig. 3 Dependence of the demodulated photoacoustic signal amplitude normalized to the incident optical intensity on the reference saturation $SatO_{2,ref}$ at the optical wavelength 650nm.

The quantitative results obtained by calibration with the first setup are depicted in Fig. 5. The photoacoustically determined values $SatO_{2,PA}$ are in good agreement with the reference values $SatO_{2,ref}$. The deviations from the ideal straight line can be explained by the limited accuracy of the reference system. The horizontal error bars in Fig. 5 are the error bars of the reference system. Comparing the photoacoustically determined oxygen saturation values to the ideal straight line results in a R^2-value of $R^2 = 0.96$. This result indicates that the photoacoustic detection offers at least accuracy comparable to the reference system.

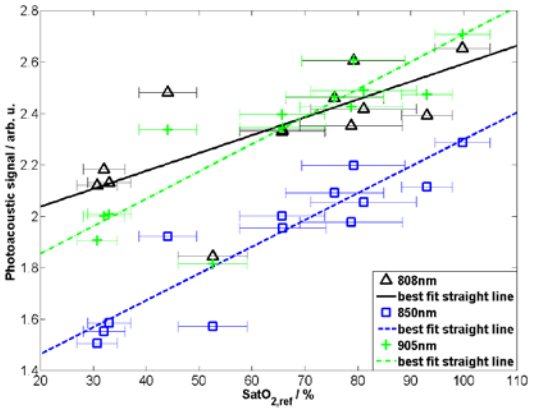

Fig. 4 Dependence of the demodulated photoacoustic signal amplitude normalized to the incident optical intensity on the reference saturation $SatO_{2,ref}$ at the optical wavelengths 808nm, 850nm and 905nm.

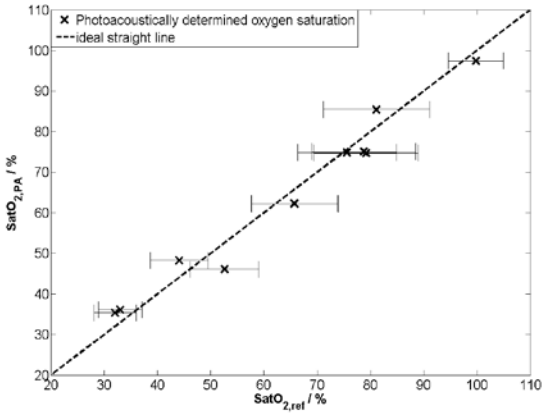

Fig. 5 Dependence of the photoacoustically determined oxygen saturation $SatO_{2,PA}$ on the reference saturation $SatO_{2,ref}$ using all four wavelengths.

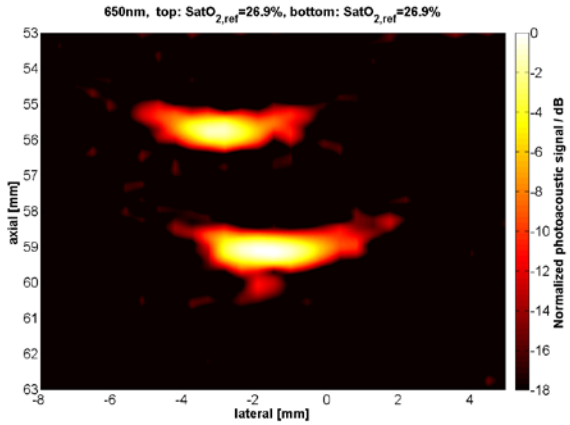

Fig. 6 Experiment 1: Normalized and interpolated photoacoustic image of the blood vessel mimicking sample filled with deoxygenated porcine blood during illumination at 650nm.

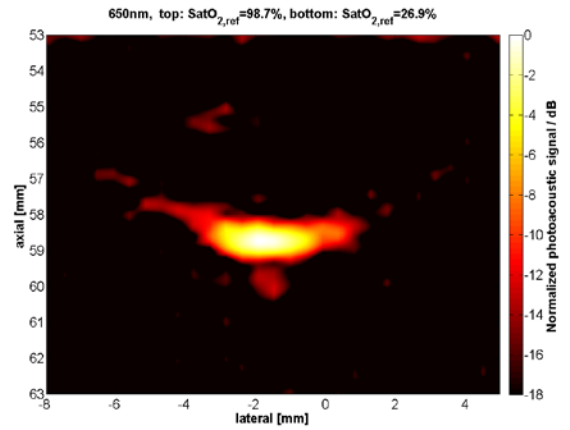

Fig. 7 Experiment 2: Normalized and interpolated photoacoustic image of the blood vessel mimicking sample filled with oxygenated (top) and deoxygenated (bottom) porcine blood during illumination at 650nm.

Fig. 6-9 show the resulting images of the blood vessel mimicking sample containing either the same blood (both tubes $SatO_{2,ref}$ = 26.9%, Experiment 1) or blood with different oxygen saturation levels (top tube $SatO_{2,ref}$ = 98.7%, bottom tube $SatO_{2,ref}$ = 26.9%, Experiment 2) for the two different wavelengths (650nm and 850nm). These images were

obtained by averaging 200 times and by using a delay-and-sum beamforming algorithm. As can be seen from Fig. 6 and Fig. 8 both wavelength beams illuminate the two tubes evenly. The tube filled with almost completely oxygenated blood disappears within the image obtained by illuminating the sample at 650nm (Fig. 9). Both tubes remain visible in the photoacoustic image by using an excitation wavelength of 850nm (Fig. 11).

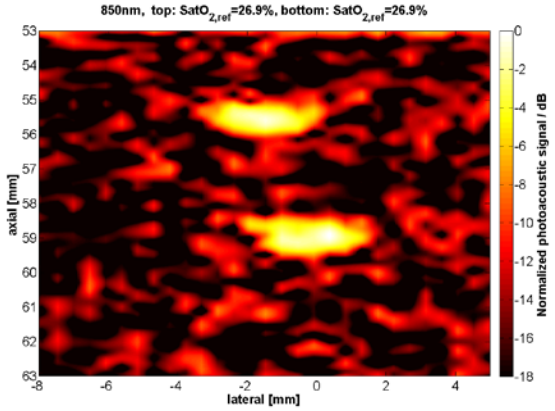

Fig. 8 Experiment 1: Normalized and interpolated photoacoustic image of the blood vessel mimicking sample filled with deoxygenated porcine blood during illumination at 850nm.

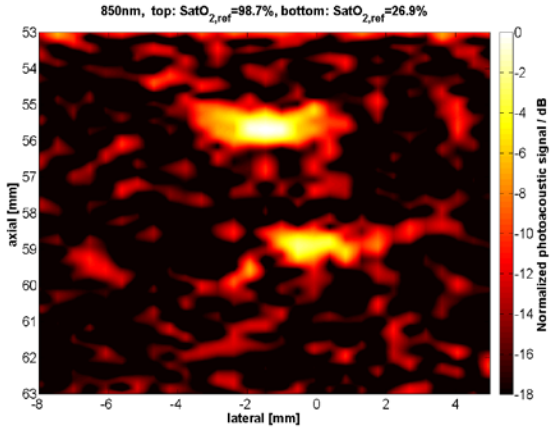

Fig. 9 Experiment 2: Normalized and interpolated photoacoustic image of the blood vessel mimicking sample filled with oxygenated (top) and deoxygenated (bottom) porcine blood during illumination at 850nm.

Due to the small tube diameter, the second step of the calibration procedure may be neglected for quantitative oxygen saturation imaging (Eq. (8)). Calculations using the absorption coefficients, the scattering coefficients and the anisotropy factor provided in [15] lead to a minimum effective optical penetration depth $\frac{1}{\mu_{\text{eff}}}$ (worst case) at 650nm of 0.393 mm for a hematocrit value of 42% (porcine blood typically possesses a hematocrit value between 30%-42% [18]) and an oxygen saturation value of 50% according to Eq. (6). The mean optical path length through a tube with a diameter of 0.45mm is 0.353mm which is comparable to the effective optical penetration depth. Therefore, the influence of scattering on the detected photoacoustic signal can be neglected as long as the blood sample is not completely deoxygenated. The resulting oxygen saturation values of each tube are shown in Fig. 10. The photoacoustically determined oxygen saturation values have been calculated from the maximum photoacoustic signal amplitude of each tube. It can be seen that the oxygen saturation values are in good agreement with the values of the reference system. Due to our approximation to neglect the scattering influence, the results at low oxygen saturation are less accurate.

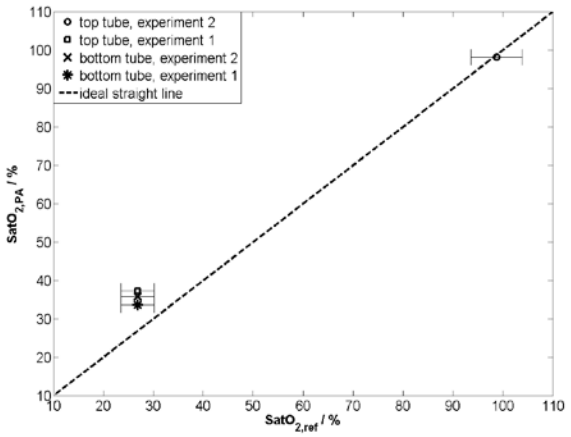

Fig. 10 Dependence of the photoacoustically determined oxygen saturation $SatO_{2,PA}$ on the reference saturation $SatO_{2,ref}$ of the two blood vessel mimicking sample experiments.

VI. CONCLUSIONS

We demonstrated that semiconductor laser systems allow for photoacoustic blood oxygenation measurements. We used porcine whole blood to emulate the behavior of human whole blood. Even though the photoacoustic signal is influenced by optical backscattering within the blood sample there was a good agreement (R^2=0.96) between the photoacoustically measured oxygen saturation values and the values determined by the reference system. Additionally, our results show that wavelengths (like 650nm) offering large differences between the optical extinction coefficients of oxygenated and deoxygenated hemoglobin are preferable to wavelengths with small differences.

Furthermore we demonstrated quantitative photoacoustic blood oxygenation imaging based on semiconductor lasers by employing a standard transducer array and by using a blood vessel mimicking sample. As at very small blood vessel diameters optical backscattering is negligible, this was possible without additional calibration. This experiment documents the ability of semiconductor lasers to be used in combination with standard ultrasound transducer arrays for biomedical imaging purposes.

In the future, semiconductor laser based photoacoustic blood oxygenation measurement systems could be a cost-effective alternative to other blood oxygenation imaging systems. As has been reported in [25] *in vivo* measurements within turbid media are more challenging, but this is a general issue which does not depend on the laser excitation system and therefore is beyond the scope of this study. Employing broad bandwidth ultrasound detectors might solve this problem by using inversion scheme approaches like, for instance, being presented in [6].

ACKNOWLEDGMENT

This project was funded by the German Federal Ministry of Education and Research (bmb+f grant no. 01 EZ 0707).

REFERENCES

[1] A. A. Tandara, and T. A. Mustoe, "Oxygen in Wound Healing – More than a Nutrient", World J. Surg. vol. 28 (3), pp. 294-300, 2004.

[2] M. F. Stiefel, A. Spiotta, V: H. Gracias, A. M. Garuffe, O. Guillamondegui, E. Maloney-Wilensky, S. Bloom, M. S. Grady, and P. D. LeRoux, "Reduced mortality rate in patients with severe traumatic brain injury treated with brain tissue oxygen monitoring", J. Neurosurg., vol. 103, pp. 805-811, 2005.

[3] I. Vanzetta, and A. Grinvald, "Increased Cortical Oxidative Metabolism Due to Sensory Stimulation: Implications for Functional Brain Imaging", Science, vol. 286, pp. 1555-1558, 1999.

[4] J. Laufer, E. Zhang, G. Raivich, and P. Beard, "Three-dimensional noninvasive imaging of the vasculature in the mouse brain using a high resolution photoacoustic scanner" J. of Appl. Opt., vol. 48 (10), pp. D299-D306, 2009.

[5] J. Laufer, C. Elwell, D. Delpy, and P. Beard, "In vitro measurements of absolute blood oxygen saturation using pulsed near-infrared photoacoustic spectroscopy: accuracy and resolution", Phys. Med. Biol., vol. 50, pp. 4409-4428, 2005.

[6] J. Laufer, D. Delpy, C. Elwell, and P. Beard, "Quantitative spatially resolved measurement of tissue chromophore concentrations using photoacoustic spectroscopy: application to the measurement of blood oxygenation and haemoglobin concentration", Phys. Med. Biol., vol. 52, pp. 141-168, 2007.

[7] I. Y. Petrova, Y. Y. Petrov, R. O. Esenaliev, D. J. Deyo, I. Cicenaite, and D. S. Prough, "Noninvasive monitoring of cerebral blood oxygenation in ovine superior sagittal sinus with novel multi-wavelength optoacoustic system", Opt. Express, vol. 17 (9), pp. 7285-7295, 2009.

[8] M. P. Mienkina, C.-S. Friedrich, N. C. Gerhardt, W. G. Wilkening, M. R. Hofmann,G. Schmitz,"Experimental Evaluation of Photoacoustic Coded Excitation using Unipolar Golay Codes", IEEE Transactions on Ultrasonics, Ferroelectrics, and Frequency Control, vol. 57 (7), pp. 1583-1593, 2010.

[9] M. P. Mienkina, C.-S. Friedrich, N. C. Gerhardt, M. F. Beckmann, M. F. Schiffner, M. R. Hofmann, G. Schmitz, "Multispectral photoacoustic coded excitation imaging using unipolar orthogonal Golay codes", Opt. Express, vol. 18 (9), pp. 9076-9087, 2010.

[10] R. G. M. Kolkman, W. Steenbergen, and T. G. van Leeuwen, "In vivo photoacoustic imaging of blood vessels with a pulsed laser diode", Lasers in medical science, vol. 21 (3), pp. 134-139, 2006.

[11] T. J. Allen, and P. C. Beard, "Dual wavelength laser diode excitation source for 2D photoacoustic imaging.", Proc. SPIE, vol. 6437, pp. 64371U-1 - 64371U-9, 2007.

[12] V. E. Gusev, and A. A. Karabutov, *Laser Optoacoustics* , American Institute of Physics, New York, USA, 1993.

[13] L. V. Wang, and H. Wu, *Biomedical Optics*, John Wiley & Sons, Inc., Hoboken, New Jersey, 2007.

[14] Z. Guo, S. Hu, and L. V. Wang, "Calibration-free absolute quantification of optical absorption coefficients using acoustic spectra in 3D photoacoustic microscopy of biological tissue", Opt. Lett., vol. 35 (12), pp. 2067-2069, 2010.

[15] D. J. Faber, M. C. G. Aalders, E. G. Mik, B. A. Hooper, M. J. C. van Gemert, and T. G. van Leeuwen, "Oxygen Saturation-Dependent Absorption and Scattering of Blood", Phys. Rev. Lett., vol. 93 (2), pp. 028102-1 – 028102-4, 2004.

[16] A. A. Oraevsky, S. L. Jacques, and F. K. Tittel, "Measurement of tissue optical properties by time-resolved detection of laser-induced transient stress", J. Appl. Opt., vol. 36 (1), pp. 402-415, 1997.

[17] G. M. Hale, and M. R. Querry, "Optical Constants of Water in the 200-nm to 200-µm Wavelength Region", J. Appl. Opt., vol. 12 (3), pp. 555-563, 1973.

[18] Walter Baumgartner, *Klinische Propädeutik der Haus- und Heimtiere*, Parey in MVS Medizinverlage Stuttgart GmbH & Co. KG, Stuttgart, Germany, 2009.

[19] W. G. Zijlstra, A. Buursma, and O. W. van Assendelft, *Visible and Near Infrared Absorption Spectra of Human and Animal Haemoglobin*, VSP BV, Utrecht, Netherlands, 2000.

[20] R. Serianni, J. Barash, T. Bentley, P. Sharma, J. L. Fontana, D. Via, J. Duhm, R. Bunger, and P.D. Mongan, "Porcine-specific hemoglobin saturation measurements", J. Appl. Physiol., vol. 94, pp. 561-566, 2003.

[21] D. C. Willford, and E. P. Hill, "Modest effect of temperature on the porcine oxygen dissociation curve", Respiration Physiology, vol. 64, pp. 113-123, 1986.

[22] G. R. Kelman, "Digital computer subroutine for the conversion of oxygen tension into saturation", J. Appl. Physiol., vol. 21 (4), pp. 1375-1376, 1966.

[23] J. W. Severinghaus, "Oxyhemoglobin Dissociation Curve Correction for Temperature and pH Variation in Human Blood", J. Appl. Physiol., vol. 12 (3), pp. 485-486, 1958.

[24] R. W. Burnett, and D. C. Noonan, "Calculations and Correction Factors Used in Determination of Blood pH and Blood Gases", Clinical Chemistry, vol. 20 (12), pp. 1499-1506, 1974.

[25] M. Sivaramakrishnan, K. Maslov, H. F. Zhang, G. Stoica, and L. V. Whang, "Limitations of quantitative photoacoustic measurements of blood oxygenation in small vessels", Phys. Med. Biol., vol. 52, pp. 1349-1361, 2007.